



The role of clay content and mineral surface area for soil organic carbon storage in an arable toposequence

Steffen A. Schweizer · Carsten W. Mueller · Carmen Höschen · Pavel Ivanov · Ingrid Kögel-Knabner

Received: 19 May 2021 / Accepted: 1 September 2021 / Published online: 1 October 2021
© The Author(s) 2021

Abstract Correlations between organic carbon (OC) and fine mineral particles corroborate the important role of the abundance of soil minerals with reactive surfaces to bind and increase the persistence of organic matter (OM). The storage of OM broadly consists of particulate and mineral-associated forms. Correlative studies on the impact of fine mineral soil particles on OM storage mostly combined data from differing sites potentially confounded by other environmental factors. Here, we analyzed OM storage in a soil clay content gradient of 5–37% with similar farm management and mineral composition. Throughout the clay gradient, soils contained 14 mg OC g⁻¹ on average in the bulk soil without showing any systematic increase.

Density fractionation revealed that a greater proportion of OC was stored as occluded particulate OM in the high clay soils (18–37% clay). In low clay soils (5–18% clay), the fine mineral-associated fractions had up to two times higher OC contents than high clay soils. Specific surface area measurements revealed that more mineral-associated OM was related to higher OC loading. This suggests that there is a potentially thicker accrual of more OM at the same mineral surface area within fine fractions of the low clay soils. With increasing clay content, OM storage forms contained more particulate OC and mineral-associated OC with a lower surface loading. This implies that fine mineral-associated OC storage in the studied agricultural soils was driven by thicker accrual of OM and decoupled from clay content limitations.

Responsible Editor: Stuart Grandy.

Supplementary Information The online version contains supplementary material available at <https://doi.org/10.1007/s10533-021-00850-3>.

S. A. Schweizer (✉) · C. W. Mueller · C. Höschen · I. Kögel-Knabner
Soil Science, TUM School of Life Sciences, Technical University of Munich, Emil-Ramann-Str. 2, 85354 Freising-Weihenstephan, Germany
e-mail: schweizer@soil-science.org

Present Address:
C. W. Mueller
Department of Geosciences and Natural Resource Management, University of Copenhagen, Øster Voldgade 10, 1350 Copenhagen K, Denmark

Keywords Soil organic matter · Fine mineral particles · Organic carbon storage · Clay content ·

P. Ivanov
Hydrogeology, Institute of Geosciences, Friedrich-Schiller-University Jena, Burgweg 11, 07749 Jena, Germany

I. Kögel-Knabner
Institute for Advanced Study, Technical University of Munich, Lichtenbergstraße 2a, 85748 Garching, Germany

Organic carbon loading · Nanoscale secondary ion mass spectrometry

Introduction

There is considerable debate about the factors and mechanisms responsible for OM storage in soils. Soils harbor more carbon worldwide than is stored in both the phytomass and the atmosphere (Scharlemann et al. 2014; Sulman et al. 2018). In particular, the potential of agricultural soils to sequester carbon has been recently discussed under the notion of climate change mitigation (Mayer et al. 2018; Loisel et al. 2019; Bossio et al. 2020). Interactions between soil organic carbon (OC) and mineral soil particles reduce the accessibility of OC for degraders, governing its susceptibility to mineralization and release into the atmosphere (Torn et al. 1997; Schmidt et al. 2011; Kleber et al. 2015, 2021). Fine mineral soil particles and aggregated soil structures exert control over OC content through sorption of organic matter (OM) at mineral surfaces and occlusion in aggregates, protecting particulate OM and its decomposition products from further degradation (Jones and Edwards 1998; Baldock and Skjemstad 2000; Schmidt et al. 2011; Cotrufo et al. 2015). Across various soils, correlations of the OC content with the mass proportion of fine mineral particles in the clay and silt size range have led to the adoption of fine mineral particles as a proxy for OM storage in current conceptual frameworks and modelling efforts on the soil OC cycling (Campbell and Paustian 2015; Bailey et al. 2018). However, direct evidence relating OM storage to mineral surface area is often lacking.

Most studies that link OC content to the mass proportion of fine mineral soil particles include samples across large scales, including varying climates, land use, soil types and soil depths. Climatic conditions were found to affect the relationship between OC stocks and clay content (Zhong et al. 2018). Such diverse interrelations between environmental site factors could confound the effects of fine particles on OC storage since many of these factors are often cross-correlated with each other and the clay content. Controlling for such site factors may make the

analysis of assessing the influence of fine mineral particles on OM storage more accurate.

A compelling number of studies assume the capacity of soils to store OM to be determined largely by the mass proportion of fine mineral particles with high surface area like phyllosilicates and Fe/Al (hydr)oxides (Oades 1988; Mayer 1994; Christensen 1996; Hassink 1997; Carter et al. 2003; Stewart et al. 2007; Castellano et al. 2015). This has led to the notion that soils with higher contents of fine mineral surfaces exhibit a higher potential to stabilize OM (Stewart et al. 2007; Feng et al. 2014). The association of OM with minerals, especially fine mineral particles, is related with a long-term stabilization of OM (Six et al. 2002; Cotrufo et al. 2015). According to a recent study, reactive mineral surfaces can selectively determine storage and chemical composition of OM, also termed as ‘mineral filter’ (Mikutta et al. 2019). A greater abundance of fine mineral particles can also enhance soil aggregation (Amézketa 1999; Schweizer et al. 2019) and lead to an increased stabilization of plant residues (Golchin et al. 1994a; Baldock and Skjemstad 2000; von Lützow et al. 2007). The occlusion of partly decomposed plant residues in aggregates can preserve them in a particulate form as have been isolated using density fractionation (Baldock et al. 1992; Golchin et al. 1994b; Jastrow 1996; Baldock and Skjemstad 2000; Wagai et al. 2009b). Due to the enhancement of soil aggregation by fine mineral particles and their reported influences on OM storage within aggregates (Balabane and Plante 2004; Schweizer et al. 2019), the occlusion of particulate OM and physical protection may increase the storage of OC in these forms. Since fine mineral particles were reported to foster both mineral-associated OM and particulate OM (Plante et al. 2006), there is a need to differentiate these OM storage forms systematically. Fractionation of mineral-associated and particulate forms may enable a better understanding of how the abundance of fine mineral particles is affecting the division of OM in different storage forms. Further information on the storage form of OM has critical implications in light of climate change scenarios that advocate efforts for increased soil carbon sequestration, especially in arable soils (Chabbi et al. 2017; Bailey et al. 2018).

The effect of fine mineral particles on the storage of OM is often assumed to be controlled by their high mineral surface area to associate with OM (Mayer

1994; Hassink 1997; Wiseman and Puttmann 2005). The binding of a specific amount of OM per mineral surface area, measured as OC loading, was used to explain the positive correlation of fine mineral particles and stored OM in soils (Kahle et al. 2002; Séquaris et al. 2010; Feng et al. 2013). Moreover, sorption experiments using phyllosilicates and (oxyhydr)oxides have shown that the relationship between the content of sorbed OC and mineral surface area is non-linear (Kaiser and Guggenberger 2003). A recent comparison of a forest soil with an agricultural soil in the US showed that an equal mineral surface area was covered by OM in the top 15 cm despite two times higher OC contents in the bulk soil under forest (Wang et al. 2019). These uncertainties in the relationship of mineral surface area and OC content in soils indicate that the roles of mineral surface area and the associated OC loading need to be elucidated when relating OM storage with fine mineral particles. The quantification of the OC loading is helpful to determine to which extent the impact of fine mineral particles on the OM storage is related to the mineral surface area.

In this study, we took topsoil samples from an agricultural experimental site with similar management but a wide range of clay content (5–37%). Across the clay content gradient, we investigated how differences in clay content affect OC content and proportions of particulate and mineral-associated forms. This enabled us to constrain how OM is allocated across mineral surfaces of fine mineral particles. We analyzed the specific surface area and amount of OM on the mineral surface by N₂-adsorption before and after OM removal to quantify the OC loading. We also quantified the microscale arrangement of mineral-associated OM using nanoscale secondary ion mass spectrometry (NanoSIMS) (Herrmann et al. 2007; Keiluweit et al. 2012; Mueller et al. 2013). Based on the distribution of ¹²C⁻, ¹²C¹⁴N⁻ (indicative for OM) and ¹⁶O⁻ (indicative for mineral surfaces), we quantified the distribution of OM on the projected surface at the microscale using automatic image analysis by multichannel machine-learning (Schweizer et al. 2018). We hypothesized that soils with lower clay content contain less mineral-associated OM due to lower proportions of fine mineral particles and associated mineral surface area. We also hypothesized that higher content of mineral-associated OM is related to a larger proportion of the mineral surface area associated with OC. Using this approach, we aimed to

unravel the impact of fine mineral particles on mineral-associated and particulate storage forms of OM in soil.

Material and methods

Field experiment and site

To elucidate the impact of soil particle size distribution on OM allocation, we selected a site with similar farm management practices and parent material at the research station in Scheyern, located 40 km north of Munich (Germany), as described by Kölbl and Kögel-Knabner (2004) and Krause et al. (2018). The annual mean temperature at the sampling site is 7.4 °C with an average annual precipitation of 803 mm at 445 to 498 m above sea level. The parent material is Miocene Upper Freshwater Molasse, a typical sediment in the North Alpine foreland basin, heterogeneously covered by Quaternary loess. Accordingly, the wide variation of clay contents were likely related to the riparian sedimentation dynamics of the Upper Freshwater Molasse, a varying thickness of Loess depositions and the later homogenization of these parent materials through agricultural management (e.g. plowing). The soils at the sampling site are classified as an association of Cambisols and Luvisols according to the World Reference Base for Soil Resources. All soils were decalcified with typical pH values of 5.2–5.8 on average (Kölbl and Kögel-Knabner 2004; Schweizer et al. 2019) and no evidence of lime applications was found in the samples.

The soil samples were all taken from the same experimental farm with a history of decades of intensive agricultural usage (Schröder et al. 2002). After 1992, the land management practice was changed to harrowing and chisel plowing instead of moldboard plowing. The sites received synthetic N fertilizer and cattle manure. As reported in Schweizer et al. (2019) based on a remote sensing study (Sommer et al. 2003), soils at the site with a clay content of 19–22% received approximately 11% less C input from wheat harvest residues than soils with a clay content of 32–34%.

Sampling sites at the experimental farm were determined to systematically represent increment ranges of clay content along the clay gradient based on previous remote sensing studies (Sommer et al.

2003; Weller et al. 2007). In total, 56 sites with a clay content gradient of 5–37% of the experimental farm were sampled from the top 20 cm of soil. Subsets of the gradient were analyzed in previous works as referenced respectively. The clay content values of 25 of these sites (with a range of clay content of 16–37%) were taken over from Krause et al. (2018). The clay content values of the remaining sites (with a range of clay content between 5 and 33%) were taken over from Kölbl and Kögel-Knabner (2004) and had a large overlap with the clay content of the other sites. Overall, the 56 sampling sites were gathered across an area of approximately 6 ha with a distance of approximately 15–50 m between each of them.

The top 5 cm was discarded to avoid the influence of crust formation and slaking at 25 sites with a clay content ranging between 16–37% that were used for < 250 µm aggregate size distribution analyses for a previous study (Schweizer et al. 2019). Since the fields were regularly plowed, we assumed that the remaining material after removal of the top 5 cm was representative of the whole Ap horizons. The field fresh soil samples were sieved (< 8 mm mesh) and stored at 4 °C for the combined density and size fractionation. Soil material for the other analyses of clay content and bulk OC content was air-dried.

Clay content and mineral composition

The topsoil samples showed a wide variety of clay content from 5 to 37% at a consistent pH of 5.9. After air drying, the samples for clay and mineralogical analysis all samples were treated with an excess of 30% H₂O₂ to remove OM and wet sieved to 63–2000 µm and < 63 µm. In the < 63 µm fraction, the silt and clay content was determined by X-ray attenuation using a Sedigraph (Micromeritics, Georgia, USA).

To determine whether the clay mineralogical composition changed across the clay gradient, we fractionated the clay-sized particles (< 2 µm) of soils with 16–37% clay by sedimentation and saturated them with Mg²⁺ and K⁺. The X-ray diffraction patterns at 3–32° 2Theta were measured using a Bruker D8 Advance (Bruker, Billerica, USA). The Mg-saturated samples were then saturated with ethylene glycol. The K-saturated samples were heated stepwise to 400 °C and 550 °C. The relative content of clay minerals was assessed using the ratio between the

areas of the characteristic reflexes, considering their corresponding weight factors (Biscaye 1965). We found a clay mineral composition that was dominated by illite, with a low kaolinite and chlorite content (Table S1). There were minor (low to moderate) differences between samples in the content of expansive clay minerals like smectite and vermiculite (Table S1). As well as quartz, traces of K- and Na-feldspars were found. Among these minor differences of clay mineral composition, we did not observe any systematic increase or decrease of a certain clay mineral with clay content.

To determine Fe and Al (oxyhydr)oxides, we used two chemical extractions performed in a sequential manner (Heckman et al. 2018). We first extracted mineral fractions using acid ammonium oxalate extraction (oxalate), which is assumed to target short-range-order and other non-crystalline phases (Schwertmann 1964). Afterwards, we used a dithionite-citrate-bicarbonate (DCB) to extract remaining crystalline Fe and Al oxides.

For the extraction with oxalate at pH 3 (Schwertmann 1964), we added approximately 1 g of bulk soil to a centrifuge tube. After adding 30 ml of oxalate, we vortexed the tubes for 20 s and shook them for 2 h in the dark. Next, we centrifuged each sample for 20 min at 20,000 g. The supernatant was filtered through a syringe-tip filter (0.2 µm, RC, Phenomenex®). Subsequently, we added approximately 40 ml of deionized H₂O and vortexed and centrifuged the sample two times as described to remove remaining Fe and Al in the extractant. After washing of the residual soil material, we performed the second extraction with 30 ml of DCB at pH 7 following Mehra and Jackson (1958). After vortexing and 16 h shaking, we centrifuged and filtered the samples as described previously. Next, we analyzed the Fe and Al contents in the extract with inductively coupled plasma optical emission spectroscopy (ICP-OES; Vista-Pro, Varian, USA). Increasing proportions of Fe and Al (oxyhydr)oxides extractable by oxalate were found to be in line with increasing clay content (Fig. S3). The oxalate extract is assumed to target non-crystalline phases, which provide a high potential for association with OM (Mikutta et al. 2006). Across the clay content gradient, the silt content and Fe and Al (oxyhydr)oxides increased linearly with clay content, whereas the sand content decreased. The clay content is, therefore,

used as a proxy for fine and reactive mineral particles in this work, as also proposed by Churchman (2010).

Physical fractionation and carbon and nitrogen analyses

All soil samples were fractionated using a combined density and size fractionation described by Kölbl and Kögel-Knabner (2004). The free particulate OM fraction was obtained in a sodium polytungstate solution of 1.8 g cm^{-3} and the occluded particulate OM was extracted after additional sonication at 500 J cm^{-3} . All fractions were washed with deionized H_2O using pressure filtration to $< 1 \mu\text{S cm}^{-1}$. To obtain the mineral-associated OM fractions, the particles $> 1.8 \text{ g cm}^{-3}$ were fractionated by sieving into the size fractions $< 20 \mu\text{m}$, $20\text{--}200 \mu\text{m}$ and $200\text{--}2000 \mu\text{m}$. From the $< 20 \mu\text{m}$ fraction we obtained the fine fractions $< 2 \mu\text{m}$, $2\text{--}6.3 \mu\text{m}$ and $6.3\text{--}20 \mu\text{m}$ using sedimentation. The $< 2 \mu\text{m}$ fraction was further split into $< 0.2 \mu\text{m}$ and $0.2\text{--}2 \mu\text{m}$ fractions using centrifugation. Scanning electron microscopy analyses of the fine fractions obtained by sedimentation exhibited larger diameters than expected. This can be explained by the non-spherical structure of particles and aggregates in these fractions and varying densities due to associated OM (Konert and Vandenberghe 1997; Laird 2001). All mineral-associated fractions were freeze-dried. The carbon and nitrogen contents of the bulk soil $< 2 \text{ mm}$ and the particulate OM and mineral-associated fractions were measured by dry combustion at $1000 \text{ }^\circ\text{C}$ using a Vario EL CN analyzer (Elementar, Langensfeld, Germany). The average degree of OC recovery, computed as a proportion of the recovered sum of OC in particulate and mineral-associated fractions in relation to the bulk soil OC content, is $87.7 \pm 2 \text{ s. e. } \%$ throughout the clay content gradient. This is within a typical range, as e.g. Baisden et al. (2002) reported $89 \pm 5\%$, Chenu and Plante (2006) reported $81\text{--}88\%$ and Plaza et al. (2019) reported $77\text{--}86.3\%$. Potential redistribution of particulate OM into mineral-associated fine fractions after physical fractionation was minimal as shown by C:N ratios of $8\text{--}9.5$ of OM in mineral-associated fractions. The particulate OM had a greater C:N ratio of 18.3 on average (Fig. 1d, f), which indicates highly microbially processed OM (Baldock et al. 1997; Helfrich et al. 2006). This confirms that the distribution of mineral-associated

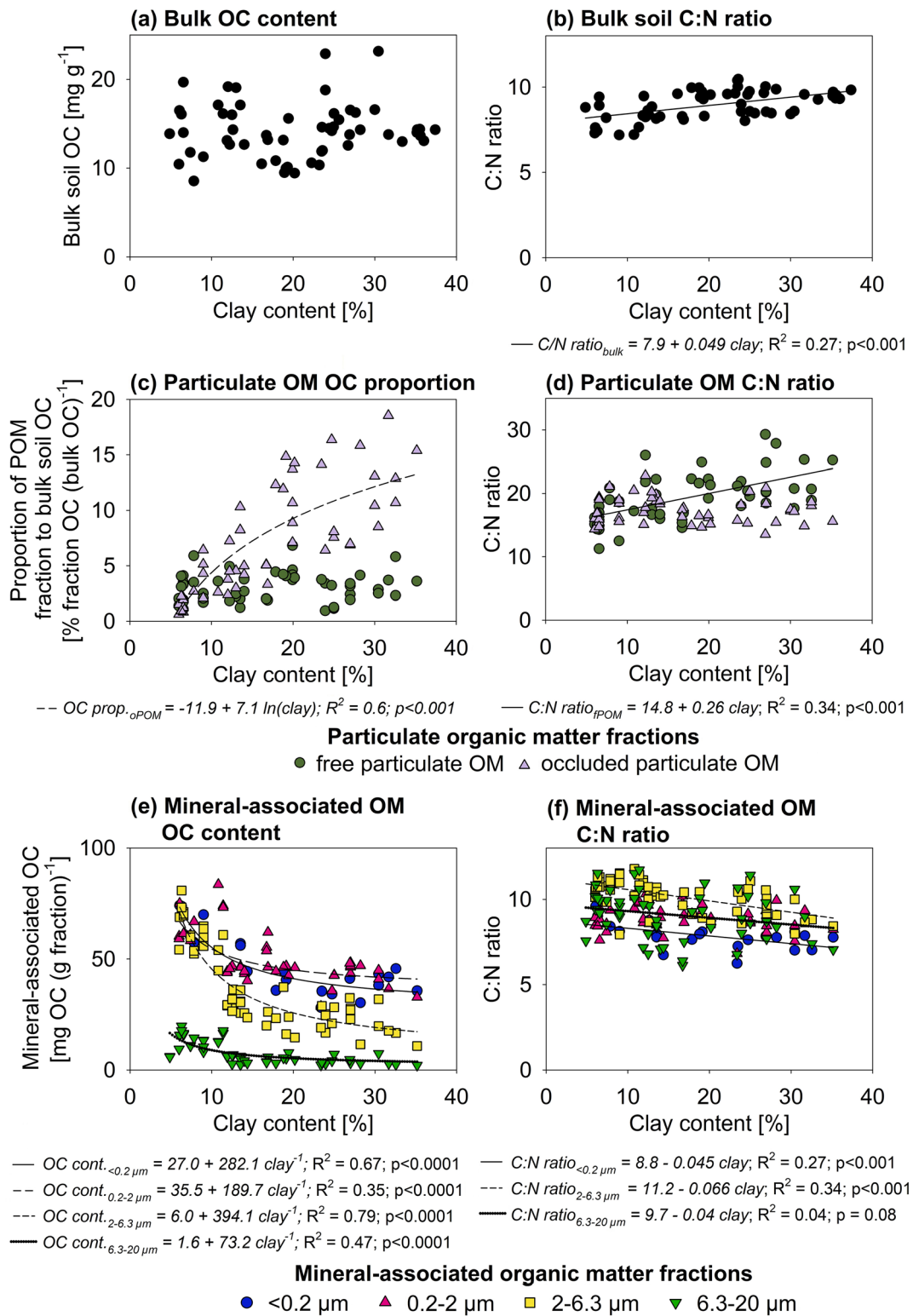
OM in fine fractions remained largely unaffected by potential artifacts during physical fractionation.

The OC stocks were calculated by the OC contents and the bulk density for the top 20 cm of fine earth $< 2 \text{ mm}$, corrected for the soil skeleton content $> 2 \text{ mm}$ and normalized according to the recovered sum of OC. The radiocarbon signature of eight representative samples (representative of the clay content gradient with OC contents close to the mean contents at the respective clay contents) was determined using accelerator mass spectrometry by Beta Analytic (Miami, USA). Since all samples were free of carbonates, they were combusted without any pretreatment. We calculated the $\Delta^{14}\text{C}$ of the samples as a relative difference of the $^{14}\text{C}:^{12}\text{C}$ ratio to that of the oxalic acid standard rate of decay after correction for the mass-dependent fractionation of ^{14}C by $\delta^{13}\text{C}$ (Stuiver and Polach 1977; Trumbore 2009). The standard was corrected for its decay between 1950 and the year of measurements in 2017, whereas the sampling dates are provided along the data in Table S2 and were considered when interpreting the data. The measurement precision of the $\Delta^{14}\text{C}$ values was 4.1% on average. The chemical composition of OM in the coarse clay-sized and the fine silt-sized was determined using solid-state ^{13}C NMR spectroscopy. A Bruker DSX 200 NMR spectrometer (Bruker, Billerica, USA) was used at a resonance frequency of 50.3 MHz with the cross-polarization magic angle spinning technique (CP-MAS). The spinning frequency was 6.8 kHz , and the samples were measured with a pulse delay of 400 ms .

Specific surface analysis with N_2 -BET

The SSA of selected mineral-associated OM fractions was determined by multi-point BET (Brunauer et al. 1938) using an Autosorb-1 analyzer (Quantachrome, Syosset, USA) with nitrogen gas as the adsorbate at 77 K . Before analysis, the samples were outgassed for 12 h under vacuum using helium at $40 \text{ }^\circ\text{C}$. Samples were measured two times with N_2 -BET and the mean of these two measurements is reported for each replicate.

To quantify the OC loading as a measure for the mineral surface area associated with OM, we used the difference of SSA before and after OM removal since the inherent OM at soil particles is known to have a low N_2 surface area (Theng et al. 1999; Kaiser and



◀ **Fig. 1** Impact of clay content on distribution of organic carbon (OC) in soil density and size fractions. **a** Bulk organic carbon (OC) content and **b** C:N ratio of the whole soil. **c** OC proportion to the bulk soil OC and **d** C:N ratio of particulate OM fractions ($< 1.8 \text{ g cm}^{-3}$). Some data for (a,b) was adapted from Schweizer et al. (2019) and for **a–d** was adapted from Kölbl and Kögel-Knabner (2004). **e** OC content of mineral-associated OM fractions and **f** C:N ratio of mineral-associated OM in fine mineral particle fractions ($> 1.8 \text{ g cm}^{-3}$). Regression models were fitted when $p < 0.05$. For more information on the proportion of mineral-associated OC to the bulk soil OC, the mass proportions of the mineral-associated fractions and the relation of the SSA to the loaded OC see Fig. S1

Guggenberger 2007; Heister 2014). To correct for the low SSA of the OM, we subtracted $1 \text{ m}^2 (\text{g OM})^{-1}$ from the measured SSA values so that they refer to the SSA of the mineral surface area not covered by OM (De Jonge and Mittelmeijer-Hazeleger 1996). The OM was removed by treating the samples with NaOCl whereas the relation of the removed OM with the associated SSA allowed us to obtain a measure of how much OM is loaded on the mineral surfaces. We treated selected mineral-associated OM fractions four times with suspensions 1:50 soil:solution of 1 M NaOCl (pH 8) for 24 h. Approximately $85 \pm 1.09 \text{ s.d.}\%$ of the OC in all samples throughout the clay content gradient was removed using this NaOCl treatment, which is coherent with previous studies (Feller et al. 1992; Mikutta et al. 2005). The degree of OC removal was consistent across both fractions and the clay content gradient in accordance with a previous study, which postulated OC removal to be unaffected by mineral surface properties and potential OM sorption mechanisms (Mikutta and Kaiser 2011). After NaOCl treatment, the soil was washed with deionized H_2O until $< 50 \mu\text{S cm}^{-1}$, freeze-dried and its SSA analyzed. The difference of the remaining N_2 -BET SSA between the untreated and the NaOCl oxidized coarse clay-sized ($0.2\text{--}2 \mu\text{m}$) and fine silt-sized ($2\text{--}6.3 \mu\text{m}$) fractions provides an estimate of the mineral surface covered by OM and the loaded OC.

To estimate a potential thickness of the loaded OC, we compared our measures with monolayer-equivalent OC loading which was established based on complex proteins like insulin or albumin (Keil et al. 1994; Mayer 1994). Such macromolecules are representative model compounds as several studies have demonstrated that mineral-associated OM is generally characterized by nitrogen-rich, proteinaceous

compounds (Kleber et al. 2007; Moon et al. 2019). The monolayer-equivalent OC loading was established based on slope calculations of the linear regression between SSA and OC content (Mayer 1994). In marine sediments and mineral soils, a monolayer-equivalent OC loading of $0.5\text{--}1 \text{ mg OC m}^{-2}$ was measured (Keil et al. 1994; Mayer 1994). This was found to represent the expected concentrations if protein-sized molecules were evenly distributed across the mineral surface. We estimated a potential thickness of the OM based on adsorbed α -synuclein and albumin which were measured to be $3\text{--}5 \text{ nm}$ thick when adsorbed (Ouberaï et al. 2014).

NanoSIMS analysis and image analysis

The coarse clay-sized fraction ($0.2\text{--}2 \mu\text{m}$) and fine silt-sized fraction ($2\text{--}6.3 \mu\text{m}$) were applied to an Si wafer as a 0.1 g l^{-1} water suspension and dried in the desiccator at room temperature (Mueller et al. 2012). We coated the samples with $\sim 5 \text{ nm}$ Au under Ar atmosphere and used secondary electron microscopy (SEM; Jeol JSM 5900) to find representative regions that contain primary particles and organo-mineral associations. After an additional Au/Pd coating of $\sim 30 \text{ nm}$ under Ar atmosphere, 5–8 regions of 7 samples representing the whole clay content gradient were analyzed with NanoSIMS 50L (Cameca, Gennevilliers, France). For that we used a Cs^+ primary ion beam with 16 keV primary ion impact energy. The primary ion current was 2 pA and the lateral resolution 150 nm. After a pre-sputtering to remove potential surface contamination and the Au/Pd coating and to reach a steady state of secondary ions, we recorded the distributions for $^{12}\text{C}_2^-$, $^{16}\text{O}^-$ and $^{12}\text{C}^{14}\text{N}^-$ (the $^{12}\text{C}^-$, $^{30}\text{Si}^-$, $^{27}\text{Al}^{16}\text{O}^-$ and $^{56}\text{Fe}^{16}\text{O}^-$ distributions were also measured but are not presented here). For each spot we recorded 40 planes with a field of view of $30 \times 30 \mu\text{m}$ with 256×256 pixels and a dwell time of 1 ms pixel^{-1} . The internal electron flood gun was used to compensate charging of soil mineral particles.

The image analysis was done according to Schweizer et al. (2018). The NanoSIMS measurements were dead-time corrected using the OpenMIMS plugin for ImageJ (Gormanns et al. 2012). After a contrast enhancement of 0.5% of the pixels (Schindelin et al. 2015), we segmented the sample images into mineral particle surfaces (indicated by the $^{16}\text{O}^-$ distribution), OM (indicated by the $^{12}\text{C}_2^-$ and $^{12}\text{C}^{14}\text{N}^-$

distributions) and background using the machine learning algorithm in Ilastik 1.2 (Sommer et al. 2011; Schweizer et al. 2018). The segmented images were used to compute the coverage of mineral particles with OM (Schweizer et al. 2018). The OM connectivity index was calculated describing, on a scale from 0 to 1, how closely the OM patches on each individual particle were connected. The OM connectivity of each particle was weighted according to the area proportion of the OM patches to the total OM area per clay content and size fraction. In total 695 particles were detected, 315 of them coated with 996 individual OM patches in 75 measurements (Table S3). To analyze the chemical composition of the OM, a normalized CN:C ratio ($^{12}\text{C}^{14}\text{N}^- : (^{12}\text{C}^{14}\text{N}^- + ^{12}\text{C}_2^-)$) was computed without previous contrast enhancement and averaged across each individual OM patch (Schweizer et al. 2018). The results of the image analysis were computed by ImageJ 1.52 and assessed with RStudio 1.3 (RStudio Team, 2020).

Statistical analysis

We used SigmaPlot 11 to test for normality (Shapiro–Wilk test) and equal variances, to fit linear regressions and to compute adjusted R^2 . The relationship between clay content and occluded particulate OC proportions was fit using a logarithmic model with the equation $f = a + b \ln(x)$ according to a previous study (Kölbl and Kögel-Knabner 2004). For the relationship between clay content and mineral-associated OC contents the best fit was found using inverse first-order regressions with the equation $f = a + b/x$ where a denotes an asymptotic minimum value of OC contents in the respective fraction under the current management conditions.

Results

Organic carbon storage in particulate and mineral-associated fractions across clay gradient

Across the wide gradient of 5–37% clay content, we found a bulk OC content of $14.2 \pm 0.4 \text{ mg OC g}^{-1}$ on average with a range of 9–23 mg OC g^{-1} not systematically related to clay contents (Fig. 1a). In the bulk soil, the C:N ratio of the OM increased from approximately 8 to 10 across the clay gradient (Fig. 1b).

Combined density and size fractionation enabled us identify clay-related changes for two major forms of OM storage, such as the particulate OM occluded in aggregates and OM associated with mineral surfaces. The results of the isolated particulate OM in low density fractions ($< 1.8 \text{ g cm}^{-3}$) revealed increasing proportions of OC in particulate OM occluded in aggregates for soils with higher clay contents (Fig. 1c). The free, non-aggregate-occluded, particulate OM contributed a proportion of 3.1% to the bulk soil OC on average throughout the clay content gradient, whereas the proportion of the occluded particulate OM increased from 0.8 to 13.3% (Fig. 1c). The C:N ratio of the free particulate OM increased linearly from 16 to 24 with increasing soil clay content whereas the C:N ratio of the occluded particulate OM showed no relationship with clay content with a mean ratio of approximately 17 (Fig. 1d).

The OC contents of the mineral-associated OM in the high-density fraction ($> 1.8 \text{ g cm}^{-3}$) followed similar decreasing trends with increasing clay content in all four mineral-associated OM fractions $< 20 \mu\text{m}$ (Fig. 1e). In both clay-sized fractions ($< 2 \mu\text{m}$) and the fine silt-sized fraction (2–6.3 μm), the mineral-associated OC was approximately 70 mg g^{-1} at 6% clay (Fig. 1e). It decreased to an asymptotic minimum value of 35.5 mg g^{-1} and 27.0 mg g^{-1} for the two clay-sized fractions (model in Fig. 1e) at clay contents of $> 30\%$. The mineral-associated OC of the fine silt-sized fraction (2–6.3 μm) decreased to even lower contents at high clay contents (empiric asymptotic value of 6 mg g^{-1}) (Fig. 1e). In the medium silt-sized fraction (6.3–20 μm), there was much less mineral-associated OC of 13.6 mg g^{-1} on average at 6% clay content decreasing to an empiric asymptotic value of 1.6 mg g^{-1} (Fig. 1e).

The C:N ratio of all mineral-associated fractions decreased with clay content by 1–2 units, except the coarse clay-sized fraction (Fig. 1f). The average C:N ratio of the fine clay-sized fraction ($< 0.2 \mu\text{m}$) was lower than both the coarse clay-sized fraction and the fine silt-sized fraction (0.2–6.3 μm) (Fig. 1f). We did not observe significant differences between different clay contents in terms of the chemical composition of OM in both the coarse clay-sized fraction and the fine silt-sized fraction according to solid-state ^{13}C nuclear magnetic resonance (NMR) (Fig. S2). The OM in these fractions is dominated by 46% O/N-alkyl C as

well as 19% alkyl C, 12% carboxyl C and 23% aryl C on average.

In the low clay soils (5–18% clay) with low proportions of particulate OC, the association with minerals accounted for up to 90% of the bulk soil OC (Fig. 2). The high proportions of the fine mineral-associated OC in the low clay soils enabled them to accommodate up to 2.7 kg OC m⁻² (at 6% clay) content associated with fine minerals in the top 20 cm (Fig. 2). In the same fraction and horizon, the high clay soils stored 1.9 kg OC m⁻² at 18–37% clay content (Fig. 2).

We observed a decrease in the radiocarbon $\Delta^{14}\text{C}$ signatures across the clay content gradient from approximately 108‰ at 6% clay content to 49‰ at 35% clay content for selected coarse clay-sized fractions (0.2–2 μm) (Table S2).

Organic matter distribution analyzed by specific surface area and NanoSIMS

Analyses of the specific surface area by N₂ sorption enabled insights into the relationship of mineral surface area with OM. The total specific surface area of the minerals after OM removal ranged from 2.4 m² g⁻¹ in the medium silt-sized fraction to 12.1 m² g⁻¹ in the fine silt-sized fraction, 37.3 m² g⁻¹ in the coarse clay-sized fraction and 80.6 m² g⁻¹ in the fine clay-sized fraction. Analyses before and after OM removal revealed that a similar specific mineral surface area was covered with OM at all clay contents (Fig. 3). The average area covered by OM was 4 times higher for the coarse clay-sized fraction (15 m² g⁻¹)

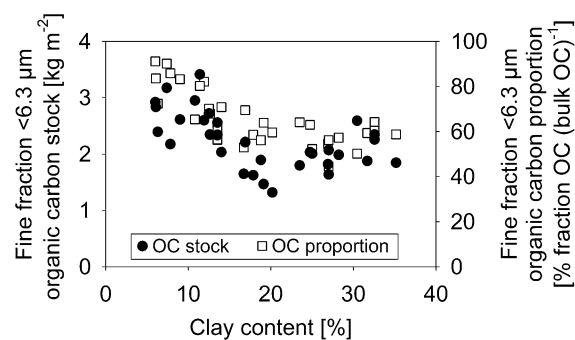


Fig. 2 Organic carbon (OC) stocks across a clay content gradient. OC stock in mineral-associated fine size fractions (> 1.8 g cm⁻³) (filled circles) in the top 20 cm and OC proportion of these fractions to the bulk soil OC (empty squares)

than for the fine-silt sized fraction (3.8 m² g⁻¹). Both fractions contained similar OC contents except for a minor difference in the high clay soils (Fig. 1e). We calculated the OC loading as amount of OC covering a certain surface area. The OC loading was approximately 5 mg OC m⁻² higher in the fine silt (7.7 mg OC m⁻²) than in the coarse clay-sized fraction (2.7 mg OC m⁻²) (Fig. 3).

We measured the distribution of OM and minerals as revealed by NanoSIMS, analyzing the elemental distributions of C, N and O in selected samples from coarse clay-sized (0.2–2 μm) and fine silt-sized (2–6.3 μm) fractions across the clay content gradient (Fig. 4). Image analysis of these measurements enabled quantification of the mean particle and OM patch size, the CN:C ratio and connectivity of OM patches as well as their coverage on the projected area of mineral-dominated surface at the microscale (Table 1). These results reflect the findings by N₂ sorption of a similar area covered by OM throughout the clay content gradient, whereas there were minor differences between the two analyzed size fractions (Table 1). Throughout the clay content gradient, 10.5 ± 0.5% of the projected mineral surface was found to be covered by OM in the coarse clay-sized

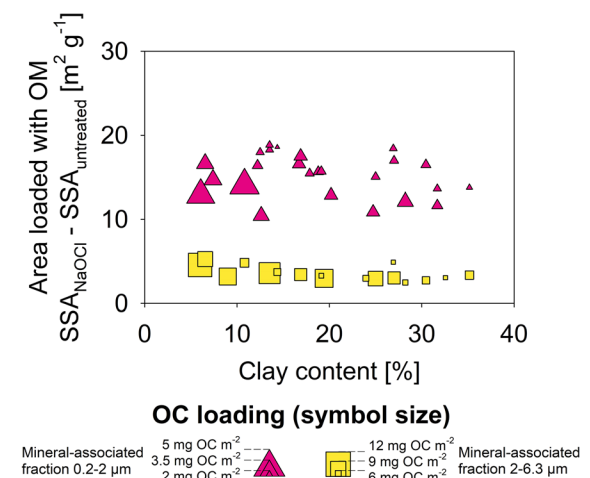
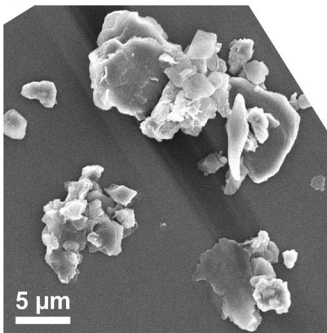


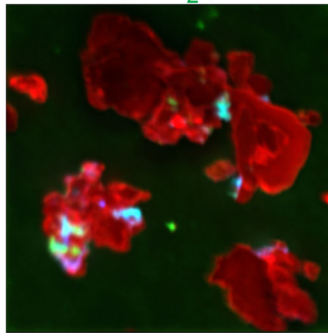
Fig. 3 Specific surface area (SSA) occupied by soil OM and loading of OC according to the symbol size (mg OC m⁻² SSA). The difference of the remaining N₂-BET SSA between the untreated and the NaOCl oxidized fractions provide a measure of the amount of OC covering a certain surface area (OC loading). The respective size of the symbols relates to the OC loading in the coarse clay-sized (0.2–2 μm) with a range of 1.7–4.7 mg OC m⁻² and the silt-sized fine fraction (2–6.3 μm) with a range of 5.5–11.8 mg OC m⁻²

Coarse clay-sized fraction (0.2–2 μm)

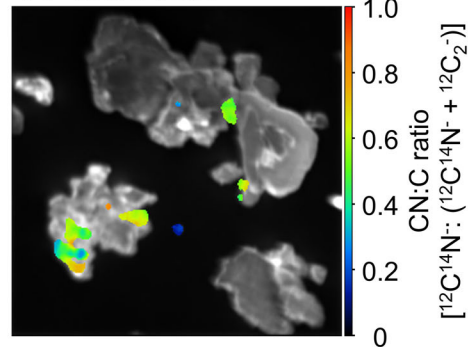
(a) SEM



(b) $^{16}\text{O}^-$, $^{12}\text{C}_2^-$, $^{12}\text{C}^{14}\text{N}^-$

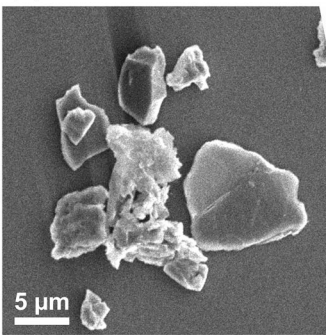


(c) CN:C ratio

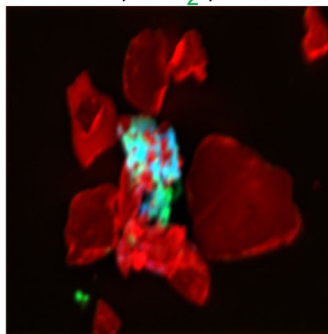


Fine silt-sized fraction (2–6.3 μm)

(d) SEM



(e) $^{16}\text{O}^-$, $^{12}\text{C}_2^-$, $^{12}\text{C}^{14}\text{N}^-$



(f) CN:C ratio

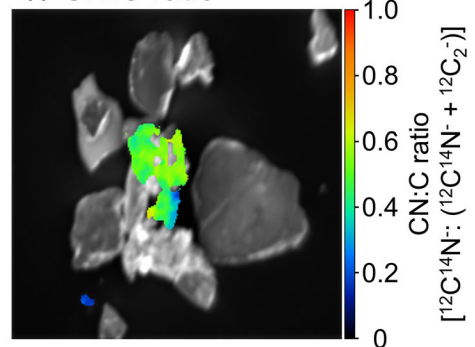


Fig. 4 Identification of organic matter distribution at micro-scale through elemental distributions. **a–c** Example measurements of the coarse clay-sized fraction (0.2–2 μm) and **d–f** of the fine silt-sized fraction (2–6.3 μm). **a, d** Scanning electron microscopy (SEM) images. **b, e** composite images of the

elemental distributions of the secondary ions $^{16}\text{O}^-$ (red), $^{12}\text{C}_2^-$ (green) and $^{12}\text{C}^{14}\text{N}^-$ (blue). (c, f) CN:C ratio ($^{12}\text{C}^{14}\text{N}^- : (^{12}\text{C}_2^- + ^{12}\text{C}^{14}\text{N}^-)$). The individual elemental distributions are shown in Fig. S4

fraction and $7.9 \pm 0.5\%$ in the fine silt-sized fraction on average (Table 1). The fine silt-sized fraction showed larger particles with a higher connectivity between the OM patches on the same particle as the coarse clay-sized fraction (Table 1). The C and N composition of OM patches at the microscale was quantified with the CN:C ratio ($^{12}\text{C}^{14}\text{N}^- : (^{12}\text{C}_2^- + ^{12}\text{C}^{14}\text{N}^-)$). On average across the clay content gradient, the OM patches in the coarse clay-sized fraction were found to exhibit a higher CN:C ratio (0.55) compared to the fine silt-sized fraction (0.44) (Table 1).

Discussion

Impact of clay content on the proportion of particulate organic matter

In contrast to established concepts linking soils with higher fine mineral surfaces to increased OM storage (Stewart et al. 2007), the arable soils that we sampled contained OC in a similar range (14.2 mg OC g^{-1} on average with a range of 9–23 mg OC g^{-1}). We did not observe any pattern of a systematic change despite a large variation in clay content ranging between 5–37% (Fig. 1a). In the high clay soils more OC is allocated to particulate OM occluded in aggregates (Fig. 1c), whereas low clay soils store almost all their OC as mineral-associated OM (Figs. 1e, 2). Although the

Table 1 Microspatial distribution properties of particles and organic matter (OM) measured by image analysis of elemental distributions

Clay content (%) and size fraction	Particles		Organic matter			Organic matter distribution	
	Total particle area analyzed (μm^2) ¹	Mean particle size (μm^2) ¹	Total OM patch area analyzed (μm^2) ¹	Mean OM patch size (μm^2) ¹	Mean CN:C ratio of OM patches ²	Total coverage (%) ³	Area-weighted connectivity of OM patches ⁴
Coarse clay-sized fraction (0.2–2 μm)							
6	1142	18 ± 4	118	2.0 ± 0.6	0.56 ± 0.03	10.3	0.51
7	1297	22 ± 6	118	1.4 ± 0.3	0.57 ± 0.02	9.1	0.69
13	1287	13 ± 1	120	0.9 ± 0.2	0.61 ± 0.02	9.3	0.55
14	1087	19 ± 7	108	1.4 ± 0.2	0.53 ± 0.03	9.9	0.54
20	2011	39 ± 12	239	2.7 ± 0.5	0.45 ± 0.02	11.9	0.49
27	1310	24 ± 9	165	1.7 ± 0.3	0.51 ± 0.02	12.6	0.43
32	2262	26 ± 6	243	2.4 ± 0.8	0.60 ± 0.03	10.7	0.56
Fine silt-sized fraction (2–6.3 μm)							
7	2114	75 ± 23	209	2.5 ± 0.9	0.46 ± 0.02	9.9	0.74
9	1030	60 ± 8	84	1.6 ± 0.5	0.49 ± 0.02	8.2	0.72
11	1245	96 ± 37	112	2.6 ± 1.2	0.50 ± 0.02	9.0	0.70
14	1743	138 ± 53	136	2.7 ± 1.6	0.48 ± 0.02	7.8	0.80
19	1839	112 ± 43	145	2.2 ± 0.9	0.44 ± 0.02	7.9	0.61
27	1761	27 ± 42	113	1.5 ± 0.4	0.42 ± 0.02	6.4	0.55
35	1816	55 ± 18	144	1.5 ± 0.6	0.30 ± 0.02	8.0	0.57

¹Particle and OM patch area and mean sizes in the coarse clay-sized fraction (0.2–2 μm) and the fine silt-sized fraction (2–6.3 μm). The total areas are sums over all areas identified as particle or OM and the mean sizes are computed as arithmetic mean and standard error

²The normalized CN:C ratio is based on the ion ratio $^{12}\text{C}^{14}\text{N}^- : (^{12}\text{C}^{14}\text{N}^- + ^{12}\text{C}_2^-)$ of the individual OM patches (mean ± standard deviation) whereas a higher CN:C ratio indicates more N-rich OM compounds

³The total coverage of OM on mineral surface is based on the summed up projected OM and particle area. Number of particles and OM patches in Table S3

⁴The dimensionless connectivity indicator was calculated per OM covered particle and area-weighted according to the area proportion of the OM patches to the total OM area

high clay soils provide more surfaces for binding OM, aggregation is likely responsible for preserving OM in particulate form in these soils at the expense of mineral-associated OM (Fig. 1c, e). This is in contrast to previous findings of more mineral-associated OM in soils with increased clay contents, and hence increased OM storage directly through binding to mineral surfaces (Stewart et al. 2007; Laganière et al. 2010; Vos et al. 2018). Instead, our results demonstrate that the occluded particulate OM pool can become increasingly important with increasing clay content.

A higher clay content may also be related to increased biomass production and interrelated OM input according to improved water availability.

However, the OC in free particulate OM was constant and did not reflect larger OM input differences. A higher OC input in the high clay soils would also be expected to lead to a higher bulk soil OC compared to the low clay soils, which was not detected. Accordingly, the increased amounts of OC in the occluded particulate OM were likely mostly attributed to the increasing stabilization through higher clay content.

The occlusion of particulate OM has been linked to encapsulating soil structures rich in clay-sized minerals which limit access for microbial degradation at the microscale (McCarthy et al. 2008; Steffens et al. 2017). Our results indicate that in soils with increased proportions of fine mineral surfaces, such as the high

clay soils of this study, increasing amounts of OM are sequestered by occlusion of particulate OM instead of being limited to association with fine mineral surfaces.

Changes of the mineral-associated organic matter fractions and C and N contents along the soil clay content gradient

While the bulk soil OC content was in a similar range across the clay gradient of 5–37% (Fig. 1a), the bulk C:N ratio increased from 8 to 10 on average (Fig. 1b). The change of the C:N ratio across the clay gradient was related to the increasing proportion of the particulate OM storage form and the decreasing mineral-associated form (Fig. 2). In the high clay soils, more occluded particulate OM (mean C:N of 17) led to an increased C:N ratio in the bulk soil. The bulk soil C:N ratio was lowest in the low clay soils, which is explained by the higher proportion of mineral-associated OM. However, the C:N ratio of the mineral-associated OM decreased with clay content (Fig. 1f). A smaller C:N ratio of the mineral-associated OM in the finer-sized fractions suggests a relation with microbial-derived OM leading to a more N-rich composition around microbial C:N ratios (Christensen 2001; von Lützow et al. 2007; Cleveland and Liptzin 2007).

The decreasing C:N ratios of OM in fine mineral-associated fractions (Fig. 1f) could also be related to a higher amount of mineral-fixed ammonium, which has been positively correlated with clay content inferring that mineral-fixed ammonium increases with higher mineral surface area (Jensen et al. 1989). However, when comparing the clay-sized and silt-sized fractions, there were no systematic differences between the C:N ratios despite large differences of the OC contents (Fig. 1e, f). This indicates that the observed C:N ratios are mostly related to the composition of mineral-associated OM and the proportion of particulate OM to the bulk soil instead of the fixation of mineral N forms. Previous studies related higher clay contents to increased association of N-rich microbial metabolites with mineral particles (Baldock et al. 1992; Baldock and Skjemstad 2000; Grandy et al. 2009; Kopittke et al. 2020). This is because microbial-derived N-rich OM is expected to be more tightly bound to mineral surfaces compared to plant-derived C-rich OM (Sollins et al. 2006, 2009; Kleber et al. 2007).

At the microscale, the CN:C ratio varied between and within individual OM patches (Fig. 4). Despite this heterogeneity, we observed a higher CN:C ratio on average indicating more N-rich OM compounds in the coarse-clay sized fraction (CN:C ratio 0.55) compared to the fine silt-sized fraction (CN:C ratio 0.44) (Table 1). This spatially explicit finding has a comparable range to the difference of the C:N ratio between the fractions measured by conventional bulk elemental analysis. This demonstrates an intimate relationship between bulk-scale measurements of the soil fractions and the elemental distributions of the projected surfaces of OM at the microscale. This supports the finding that the described properties of the OM patches, which were identified through the microscale investigation, are in line with the macroscopic OM properties in the studied fractions.

Decoupling of mineral surface area and mineral-associated organic matter content

The mineral-associated fractions < 20 μm contained higher OC contents in the soils with lower clay contents (Fig. 1e). In the low clay soils (5–18% clay), the proportion of OC associated with fine particles < 6.3 μm was high (up to 90% of bulk OC) whereas it was much lower (approximately 58%) throughout the high clay soils (18–35% clay) (Fig. 2). These results revealed that despite similarities in bulk soil OC contents across the 5–37% clay content gradient, the association of OM with minerals provided the major site for C storage in soils with lower clay contents (Figs. 1, 2). Based on these results, we rejected our initial hypothesis that a lower amount of fine mineral particles, hence less mineral surface, area would result in less mineral-associated OM in the soils.

Current understanding of soil carbon dynamics assumes that fine minerals with high surface areas preferentially retain OC in soils (Stewart et al. 2008; Feng et al. 2013). This would mean that the OC content in the clay-sized fraction would be higher than in the silt-sized fraction. Accordingly, the difference of OC contents between various fine fractions would be expected to increase when their mass proportion to the bulk soil increases. Here we show that under similar farm management practices at the same site, OC was equally retained in all mineral fractions < 6.3 μm instead of a preferential retention in the finest fractions (< 0.2 μm) (Fig. 1e). Except for a

minor difference in the high clay soils between the $< 2 \mu\text{m}$ and the $2\text{--}6.3 \mu\text{m}$ fractions, we did not observe an OM storage with preference for fine fractions (hitherto fine fractions have been presumed, to contain more reactive surface sites and OM than coarser fractions). Instead, our observations of equal OM retention in several fine mineral fractions across the clay content gradient demonstrate that OM distribution is mostly decoupled from mineral surface area (Fig. 5).

By relating specific surface area measurements with the respective OM contents of fine mineral particle fractions, we gained further insights into the mineral surface area associated with a certain amount of OM. In both the coarse clay-sized and the fine silt-sized fraction, we found that the specific surface area related with OM remained constant throughout the clay content gradient, despite the OC content almost doubling in soils with lower clay contents (Fig. 3). These results provide direct evidence of a similar area per gram fraction covered by OM throughout the clay

content gradient. In the fine silt-sized fraction, the OM occupied less surface area than in the coarse clay-sized fraction (Fig. 3), whereas the OM contents of both fractions were comparable (Fig. 1e). According to these results, we rejected our initial hypothesis that higher contents of mineral-associated OM are related to a larger extent of the mineral surface covered by OM.

Organic carbon loading of fine mineral particle fractions

Our measurements showed that a similar area per gram fine fraction was covered by mineral-associated OM (Fig. 3). Accordingly, the increasing mineral-associated OC in the low clay soils resulted in higher OC loadings (Figs. 1e, 3). A higher OC loading means that an increasing amount of OC occupies a similar mineral surface area. These results support earlier studies that also determined high OC loadings as derived from energetics of N_2 gas sorption (Wagai

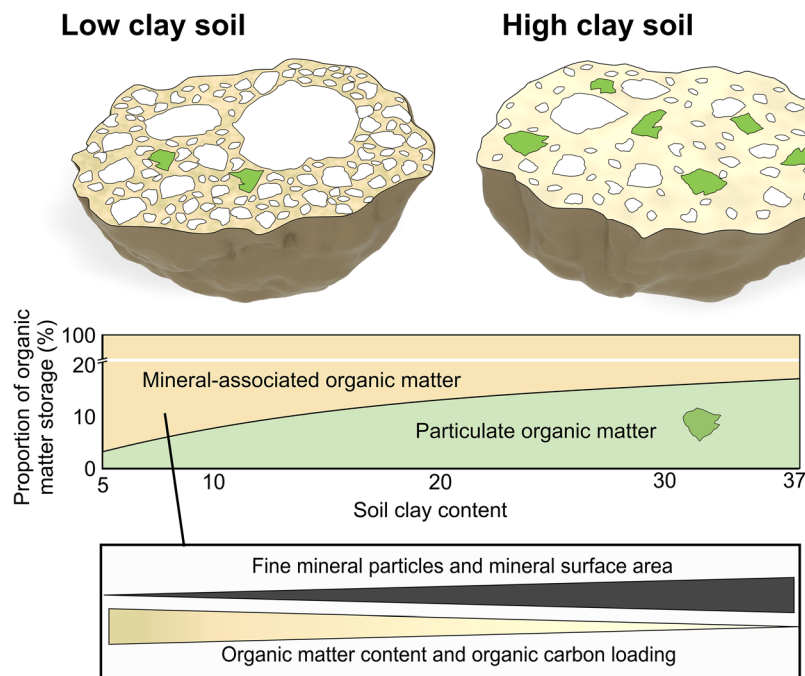


Fig. 5 Schematic overview of the OM storage in mineral-associated and particulate OM fractions across a clay content gradient of an agricultural topsoil toposequence. The OM storage was broadly divided into mineral-associated OM and particulate OM. Across the clay content gradient, the proportion of fine mineral particles that contributed to the majority of mineral surface area increased. Low clay soils are displayed

containing more large-sized mineral grains (gray) and less fine mineral particles (beige matrix). Our results indicate less particulate OM and more concentrated mineral-associated OM according to a higher OC loading in the low clay soils. In the high clay soils we found a more diluted mineral-associated OC as well as increased particulate OC

et al. 2009a) and atomic force microscopy analyses (Kaiser and Guggenberger 2007). High OC loadings imply that the OM storage is decoupled from the mineral surface area in these agricultural soils. This explains why the studied agricultural soils, even if they contain fewer fine minerals and particulate OM, can store a substantial proportion of OM through a higher OC loading (Fig. 2). Future studies should investigate to which extent the spatial arrangement of mineral-associated OM is related to mineral surface area.

We related the measurements of the OC loading with a potential thickness of the mineral-associated OM. For this, we compared our measurements with monolayer-equivalent OC loading based on proteins as representative model compounds for mineral-associated OM that is generally nitrogen-rich (Kleber et al. 2007; Moon et al. 2019). For fine-textured marine sediments and upland soils, the monolayer-equivalent OC loading was calculated at 0.5–1 mg OC m⁻² (Keil et al. 1994; Mayer 1994). With decreasing clay contents, this would mean that the OC loading in the coarse clay-sized fraction increased from approximately twofold to fourfold monolayer-equivalents and increased from sixfold to tenfold monolayer equivalents in the fine silt-sized fraction (Fig. 3). This means that the distribution of loaded OM on the mineral surface area is much greater than can be expected given monolayer arrangement. When assuming an average thickness of 3–5 nm for a protein monolayer (Ouberai et al. 2014), the thickness of the mineral-associated OM could be estimated to 6–20 nm in the coarse clay-sized fraction and 18–55 nm in the fine silt-sized fraction. If instead the OM consisted mainly of smaller organic molecules such as lipids or carbohydrates, the range of monolayer equivalents would be substantially smaller than that of proteins. Our findings of an increased storage of mineral-associated OM through higher OC loadings are in line with recent evidence and conceptual frameworks of a multilayered accumulation of OM (Possinger et al. 2020; Kleber et al. 2021).

The higher C:N ratios in the fine mineral fractions of the low clay soils of this study might also be directly related to the higher OC loading, according to the postulated zonal concept for organo–mineral associations (Sollins et al. 2006, 2009; Kleber et al. 2007). This concept describes that N-rich compounds are accumulated close to the mineral surfaces whereas

C-rich compounds are retained in the outer shell of organic coatings. Accordingly, a more C-rich composition of the mineral-associated OM in the low clay soils could be related with a higher OC loading and thicker accrual of OM. While the interrelation of measured OC loadings with monolayer equivalents provides an estimate for the potential average thickness of mineral-associated OM, the underlying structure warrants further investigation, such as the postulated assembly of organic molecular fragments at mineral surfaces (Kleber et al. 2007, 2021).

At the microscale, we discovered a high proportion of mineral surfaces that was not covered with OM accumulated in clustered patches (Fig. 4) in line with earlier observations of a patchy distribution of OM (Ransom et al. 1997; Chenu and Plante 2006). To resolve the spatial distribution of OM and minerals across the clay content gradient, NanoSIMS-based imaging allowed for the quantification of the heterogeneous spatial arrangement confined to the exposed two-dimensional surface. The total OM coverage quantified by NanoSIMS was similar throughout the clay content gradient at an average of 10.5% in the coarse clay-sized fraction (0.2–2 µm) and 7.9% in the fine silt-sized fraction (2–6.3 µm) (Table 1). This provided evidence for a constant OM coverage of mineral surfaces across the clay content gradient in line with the results from the N₂-sorption (Fig. 3).

The two-dimensional representation of the NanoSIMS-based imaging does not include the disproportionately high specific surface area of micropores that are exposed when removing OM for the N₂-adsorption measurements (Mayer and Xing 2001; Kaiser and Guggenberger 2003). This might explain the higher mineral surface area related with OM as quantified by N₂-adsorption if compared with NanoSIMS measurements. In the two-dimensional representations, 9% of the projected surfaces were covered with OM (Table 1), whereas 43 ± 2.3% of the total specific surface area probed with N₂-adsorption was covered with OM. This could be explained by intraporous occlusion of OM, whereas earlier studies showed that sorption of OM is unrealistic in pores with a diameter of < 10 nm (Mayer et al. 2004; Kaiser and Guggenberger 2007). Therefore, the specific sites of the mineral surfaces covered by OM represent a disproportionately high specific surface area.

Radiocarbon measurements of selected coarse clay-sized fractions (0.2–2 µm) showed positive Δ¹⁴C

values (47 to 115 ‰) which indicate considerable amounts of bomb C throughout all soils with differing clay contents. These measurements also demonstrate that mineral-associated OM in the coarse-clay sized fraction was turned over during a few decades or less (Table S2) (Trumbore 2009; Schrumpf and Kaiser 2015). Among the high clay soils, we observed lower $\Delta^{14}\text{C}$ values in the coarse clay-sized fraction sampled in 2015 (52‰ on average) compared to the ones sampled in 2001 (84‰ on average) which indicates that the proportion of bomb-derived ^{14}C in the coarse clay-sized fractions decreased. Accordingly, the higher values of $\Delta^{14}\text{C}$ in the low clay soils (114‰ at 7% clay content on average) would indicate a slower decrease of bomb-derived ^{14}C and OC turnover in the coarse clay-sized fraction. Relating a higher $\Delta^{14}\text{C}$ with younger OM is in line with previous works (Schrumpf et al. 2013; Mathieu et al. 2015). This would mean that the higher OC loading in the low clay soils would be related with a lower bioavailability since it might be protected from rapid decomposition. In a previous batch sorption experiment, soils with a higher hypothesized OC saturation did not stabilize less isotopically labelled OM (Feng et al. 2014). Our results on a thicker OC accrual show that this could be explained by the protection of OM depending on the OC loading of fine soil fractions. A second perspective on the observed $\Delta^{14}\text{C}$ values is that higher $\Delta^{14}\text{C}$ in the low clay soils could be related to more rapid decomposition of OM resulting in a slower dilution of bomb-derived ^{14}C in the coarse clay-sized fraction. Previous studies demonstrated that the mineral-associated OC is a mixture of younger and older components (Trumbore 1993; Swanston et al. 2005). In line with these findings, our results indicate that the OC loading of mineral-associated OM is related with its persistence over time.

Conclusions

To isolate the role of fine mineral particles in OM storage, we conducted a fractionation study of arable topsoils with a clay content gradient of 5–37%. The bulk soil contained 14 mg OC g^{-1} on average without indications of systematic changes across the clay gradient. By using density fractionation, a two-faced impact of fine mineral particles on OM storage forms, divided into mineral-associated and particulate OM,

was observed in the studied agricultural soils. In the high clay soils (18–37% clay) of this study, we found a higher proportion of OM to be stored through occlusion of particulate OM. Despite more fine mineral particles, the OM storage did not increase by association with fine mineral surfaces. The proportion of OM stored in particulate form was driven by the content of fine mineral particles. In contrast, the low clay soils (5–18% clay) contained higher proportions of their OM as mineral-associated. The OC content of the fine mineral-associated fractions in the low clay soils had up to two times higher OC contents compared to soils with higher clay content. The different impacts of fine mineral particles on the mineral-associated and particulate storage form of OM challenge univariate predictions of OM storage by mineral surface area.

Measurements of the mineral surface area related with the association of OM, by N_2 adsorption and NanoSIMS-based imaging, revealed that a similar extent of surface was related to the OM storage throughout the clay content. Accordingly, the higher mineral-associated OC content in the low clay soils was related to a more concentrated accrual of OC per mineral surface area according to our measurements of higher OC loadings. These observations indicate that the storage of mineral-associated OM was decoupled from most of the mineral surface area. The decoupled storage through increased OC loading may also impact on the thickness and turnover of mineral-associated OM necessitating further investigations. The varying thickness of mineral-associated OM accrual implies that clay content does not necessarily emerge as a limiting factor on OC uptake and storage in these agricultural soils. In future studies on soils with higher OC contents under comparable management and controlled mineral composition, we recommend to further investigate the relationship of mineral-associated OM and mineral surface area.

Acknowledgements We thank Verena Schäuble, Christian Schurig, Johann Lugmeier, Gertraud Harrington and Solvejg Roller for their technical assistance. Productive discussions with Marion Schrumpf and Werner Häusler helped us improve the manuscript. The conceptual input and comments of Angelika Kölbl on a previous version of the manuscript are gratefully acknowledged.

Author contributions S.A.S. analyzed and interpreted all data and wrote the manuscript. S.A.S., C.W.M., and I.K.K. conceptualized the study. C.H. analyzed and interpreted the NanoSIMS data while P.I. analyzed and interpreted the clay

mineral composition. All authors discussed the results and contributed to the manuscript development.

Funding We acknowledge the financial support by the Deutsche Forschungsgemeinschaft within the framework of the research unit “MAD Soil—Microaggregates: Formation and turnover of the structural building blocks of soils” (DFG RU 2179) through project KO 1035/48–1 and the NanoSIMS instrument (KO 1035/38–1). Open Access funding enabled and organized by Projekt DEAL.

Data Availability The data for Figs. and supplementary Figs. are available at <https://doi.org/10.14459/2018mp1462414>. All data generated and analyzed during this study are available from the corresponding author upon request.

Code availability Not applicable.

Declarations

Conflict of interest The authors declare no competing financial interests.

Ethical approval Not applicable.

Consent to participate Not applicable.

Consent for publication Not applicable.

Open Access This article is licensed under a Creative Commons Attribution 4.0 International License, which permits use, sharing, adaptation, distribution and reproduction in any medium or format, as long as you give appropriate credit to the original author(s) and the source, provide a link to the Creative Commons licence, and indicate if changes were made. The images or other third party material in this article are included in the article’s Creative Commons licence, unless indicated otherwise in a credit line to the material. If material is not included in the article’s Creative Commons licence and your intended use is not permitted by statutory regulation or exceeds the permitted use, you will need to obtain permission directly from the copyright holder. To view a copy of this licence, visit <http://creativecommons.org/licenses/by/4.0/>.

References

- Amézketa E (1999) Soil aggregate stability: A review. *J Sustain Agric* 14:83–151. https://doi.org/10.1300/J064v14n02_08
- Bailey VL, Bond-Lamberty B, DeAngelis K et al (2018) Soil carbon cycling proxies: understanding their critical role in predicting climate change feedbacks. *Global Change Biol* 24:895–905. <https://doi.org/10.1111/gcb.13926>
- Baisden WT, Amundson R, Cook AC, Brenner DL (2002) Turnover and storage of C and N in five density fractions from California annual grassland surface soils. *Global Biogeochem Cycles* 16:64-1-64–16. <https://doi.org/10.1029/2001GB001822>
- Balabane M, Plante AF (2004) Aggregation and carbon storage in silty soil using physical fractionation techniques. *Eur J Soil Sci* 55:415–427. <https://doi.org/10.1111/j.1351-0754.2004.0608.x>
- Baldock JA, Oades JM, Nelson PN et al (1997) Assessing the extent of decomposition of natural organic materials using solid-state ^{13}C NMR spectroscopy. *Soil Res* 35:1061–1084. <https://doi.org/10.1071/S97004>
- Baldock JA, Oades JM, Waters AG et al (1992) Aspects of the chemical structure of soil organic materials as revealed by solid-state ^{13}C NMR spectroscopy. *Biogeochemistry* 16:1–42. <https://doi.org/10.1007/bf02402261>
- Baldock JA, Skjemstad JO (2000) Role of the soil matrix and minerals in protecting natural organic materials against biological attack. *Org Geochem* 31:697–710. [https://doi.org/10.1016/S0146-6380\(00\)00049-8](https://doi.org/10.1016/S0146-6380(00)00049-8)
- Biscaye PE (1965) Mineralogy and sedimentation of recent deep-sea clay in the Atlantic ocean and adjacent seas and oceans. *Bull Geol Soc Am* 76:803–832. [https://doi.org/10.1130/0016-7606\(1965\)76\[803:MASORD\]2.0.CO;2](https://doi.org/10.1130/0016-7606(1965)76[803:MASORD]2.0.CO;2)
- Bossio DA, Cook-Patton SC, Ellis PW et al (2020) The role of soil carbon in natural climate solutions. *Nat Sustain.* <https://doi.org/10.1038/s41893-020-0491-z>
- Brunauer S, Emmett PH, Teller E (1938) Adsorption of gases in multimolecular layers. *J Am Chem Soc* 60:309–319. <https://doi.org/10.1021/ja01269a023>
- Campbell EE, Paustian K (2015) Current developments in soil organic matter modeling and the expansion of model applications: a review. *Environ Res Lett* 10:123004. <https://doi.org/10.1088/1748-9326/10/12/123004>
- Carter MR, Angers DA, Gregorich EG, Bolinder MA (2003) Characterizing organic matter retention for surface soils in eastern Canada using density and particle size fractions. *Can J Soil Sci* 83:11–23. <https://doi.org/10.4141/S01-087>
- Castellano MJ, Mueller KE, Oik DC et al (2015) Integrating plant litter quality, soil organic matter stabilization, and the carbon saturation concept. *Global Change Biol* 21:3200–3209. <https://doi.org/10.1111/gcb.12982>
- Chabbi A, Lehmann J, Ciais P et al (2017) Aligning agriculture and climate policy. *Nat Clim Chang* 7:307. <https://doi.org/10.1038/nclimate3286>
- Chenu C, Plante AF (2006) Clay-sized organo-mineral complexes in a cultivation chronosequence: revisiting the concept of the “primary organo-mineral complex.” *Eur J Soil Sci* 57:596–607. <https://doi.org/10.1111/j.1365-2389.2006.00834.x>
- Christensen BT (1996) Carbon in primary and secondary organomineral complexes. In: Carter MR, Stewart BA (eds) *Structure and organic matter storage in agricultural soils*. Lewis Publishers, Boca Raton, USA, pp 97–165
- Christensen BT (2001) Physical fractionation of soil and structural and functional complexity in organic matter turnover. *Eur J Soil Sci* 52:345–353. <https://doi.org/10.1046/j.1365-2389.2001.00417.x>
- Churchman GJ (2010) Is the geological concept of clay minerals appropriate for soil science? A literature-based and philosophical analysis Elsevier Enhanced Reader. *Phys Chem Earth* 35:927–940. <https://doi.org/10.1016/j.pce.2010.05.009>

- Cleveland CC, Liptzin D (2007) C:N: P stoichiometry in soil: is there a “Redfield ratio” for the microbial biomass? *Biogeochemistry* 85:235–252. <https://doi.org/10.1007/s10533-007-9132-0>
- Cotrufo MF, Soong JL, Horton AJ et al (2015) Formation of soil organic matter via biochemical and physical pathways of litter mass loss. *Nat Geosci* 8:776. <https://doi.org/10.1038/ngeo2520>
- De Jonge H, Mittelmeijer-Hazeleger MC (1996) Adsorption of CO₂ and N₂ on soil organic matter: nature of porosity, surface area, and diffusion mechanisms. *Environ Sci Technol* 30:408–413. <https://doi.org/10.1021/es950043t>
- Feller C, Schouller E, Thomas F et al (1992) N₂-BET specific surface areas of some low activity clay soils and their relationships with secondary constituents and organic matter contents. *Soil Sci* 153:293–299. <https://doi.org/10.1097/00010694-199204000-00005>
- Feng W, Plante AF, Aufdenkampe AK, Six J (2014) Soil organic matter stability in organo-mineral complexes as a function of increasing C loading. *Soil Biol Biochem* 69:398–405. <https://doi.org/10.1016/j.soilbio.2013.11.024>
- Feng W, Plante AF, Six J (2013) Improving estimates of maximal organic carbon stabilization by fine soil particles. *Biogeochemistry* 112:81–93. <https://doi.org/10.1007/s10533-011-9679-7>
- Golchin A, Oades JM, Skjemstad JO, Clarke P (1994a) Study of free and occluded particulate organic matter in soils by solid state ¹³C CP/MAS NMR spectroscopy and scanning electron microscopy. *Soil Res* 32:285. <https://doi.org/10.1071/SR9940285>
- Golchin A, Oades JM, Skjemstad JO, Clarke P (1994b) Soil structure and carbon cycling. *Soil Res* 32:1043–1068. <https://doi.org/10.1071/SR9941043>
- Gormanns P, Reckow S, Poczatek JC et al (2012) Segmentation of multi-isotope imaging mass spectrometry data for semi-automatic detection of regions of interest. *PLoS ONE* 7:e30576. <https://doi.org/10.1371/journal.pone.0030576>
- Grandy AS, Strickland MS, Lauber CL et al (2009) The influence of microbial communities, management, and soil texture on soil organic matter chemistry. *Geoderma* 150:278–286. <https://doi.org/10.1016/j.geoderma.2009.02.007>
- Hassink J (1997) The capacity of soils to preserve organic C and N by their association with clay and silt particles. *Plant Soil* 191:77–87
- Heckman K, Lawrence CR, Harden JW (2018) A sequential selective dissolution method to quantify storage and stability of organic carbon associated with Al and Fe hydroxide phases. *Geoderma* 312:24–35. <https://doi.org/10.1016/j.geoderma.2017.09.043>
- Heister K (2014) The measurement of the specific surface area of soils by gas and polar liquid adsorption methods—Limitations and potentials. *Geoderma* 216:75–87. <https://doi.org/10.1016/j.geoderma.2013.10.015>
- Helfrich M, Ludwig B, Buurman P, Flessa H (2006) Effect of land use on the composition of soil organic matter in density and aggregate fractions as revealed by solid-state ¹³C NMR spectroscopy. *Geoderma* 136:331–341. <https://doi.org/10.1016/j.geoderma.2006.03.048>
- Herrmann AM, Ritz K, Nunan N et al (2007) Nano-scale secondary ion mass spectrometry — A new analytical tool in biogeochemistry and soil ecology: a review article. *Soil Biol Biochem* 39:1835–1850. <https://doi.org/10.1016/j.soilbio.2007.03.011>
- Jastrow JD (1996) Soil aggregate formation and the accrual of particulate and mineral-associated organic matter. *Soil Biol Biochem* 28:665–676. [https://doi.org/10.1016/0038-0717\(95\)00159-X](https://doi.org/10.1016/0038-0717(95)00159-X)
- Jensen ES, Christensen BT, Sørensen LH (1989) Mineral-fixed ammonium in clay- and silt-size fractions of soils incubated with ¹⁵N-ammonium sulphate for five years. *Biol Fertility Soils* 8:298–302. <https://doi.org/10.1007/bf00263158>
- Jones DL, Edwards AC (1998) Influence of sorption on the biological utilization of two simple carbon substrates. *Soil Biol Biochem* 30:1895–1902. [https://doi.org/10.1016/S0038-0717\(98\)00060-1](https://doi.org/10.1016/S0038-0717(98)00060-1)
- Kahle M, Kleber M, Jahn R (2002) Carbon storage in loess derived surface soils from Central Germany: Influence of mineral phase variables. *J Plant Nutr Soil Sci* 165:141–149. [https://doi.org/10.1002/1522-2624\(200204\)165:2%3C141::AID-JPLN141%3E3.0.CO;2-X](https://doi.org/10.1002/1522-2624(200204)165:2%3C141::AID-JPLN141%3E3.0.CO;2-X)
- Kaiser K, Guggenberger G (2003) Mineral surfaces and soil organic matter. *Eur J Soil Sci* 54:219–236. <https://doi.org/10.1046/j.1365-2389.2003.00544.x>
- Kaiser K, Guggenberger G (2007) Sorptive stabilization of organic matter by microporous goethite: Sorption into small pores vs. surface complexation. *Eur J Soil Sci* 58:45–59. <https://doi.org/10.1111/j.1365-2389.2006.00799.x>
- Keil RG, Tsamakidis E, Fuh CB et al (1994) Mineralogical and textural controls on the organic composition of coastal marine sediments: Hydrodynamic separation using SPLITT-fractionation. *Geochim Cosmochim Acta* 58:879–893. [https://doi.org/10.1016/0016-7037\(94\)90512-6](https://doi.org/10.1016/0016-7037(94)90512-6)
- Keiluweit M, Bougoure JJ, Zeglin LH et al (2012) Nano-scale investigation of the association of microbial nitrogen residues with iron (hydr)oxides in a forest soil O-horizon. *Geochim Cosmochim Acta* 95:213–226. <https://doi.org/10.1016/j.gca.2012.07.001>
- Kleber M, Bourg IC, Coward EK et al (2021) Dynamic interactions at the mineral–organic matter interface. *Nat Rev Earth Environ*. <https://doi.org/10.1038/s43017-021-00162-y>
- Kleber M, Eusterhues K, Keiluweit M et al (2015) Mineral-organic associations: formation, properties, and relevance in soil environments. *Adv Agron* 130:1–140. <https://doi.org/10.1016/bs.agron.2014.10.005>
- Kleber M, Sollins P, Sutton R (2007) A conceptual model of organo-mineral interactions in soils: self-assembly of organic molecular fragments into zonal structures on mineral surfaces. *Biogeochemistry* 85:9–24. <https://doi.org/10.1007/s10533-007-9103-5>
- Kölbl A, Kögel-Knabner I (2004) Content and composition of free and occluded particulate organic matter in a differently textured arable Cambisol as revealed by solid-state ¹³C NMR spectroscopy. *J Plant Nutr Soil Sci* 167:45–53. <https://doi.org/10.1002/jpln.200321185>
- Konert M, Vandenberghe JEF (1997) Comparison of laser grain size analysis with pipette and sieve analysis: a solution for the underestimation of the clay fraction. *Sedimentology*

- 44:523–535. <https://doi.org/10.1046/j.1365-3091.1997.d01-38.x>
- Kopittke PM, Dalal RC, Hoeschen C et al (2020) Soil organic matter is stabilized by organo-mineral associations through two key processes: The role of the carbon to nitrogen ratio. *Geoderma* 357:113974. <https://doi.org/10.1016/j.geoderma.2019.113974>
- Krause L, Rodionov A, Schweizer SA et al (2018) Microaggregate stability and storage of organic carbon is affected by clay content in arable Luvisols. *Soil Tillage Res* 182:123–129. <https://doi.org/10.1016/j.still.2018.05.003>
- Laganière J, Angers DA, Paré D (2010) Carbon accumulation in agricultural soils after afforestation: A meta-analysis. *Global Change Biol* 16:439–453. <https://doi.org/10.1111/j.1365-2486.2009.01930.x>
- Laird D (2001) Nature of clay-humic complexes in an agricultural soil: II. Scanning electron microscopy analysis. *Soil Sci Soc Am J* 65:1419–1425
- Loisel J, Casellas Connors JP, Hugelius G et al (2019) Soils can help mitigate CO₂ emissions, despite the challenges. *Proc Natl Acad Sci USA* 116:10211–10212. <https://doi.org/10.1073/pnas.1900444116>
- Mathieu JA, Hatté C, Balesdent J, Parent É (2015) Deep soil carbon dynamics are driven more by soil type than by climate: a worldwide meta-analysis of radiocarbon profiles. *Glob Change Biol* 21:4278–4292. <https://doi.org/10.1111/gcb.13012>
- Mayer A, Hausfather Z, Jones AD, Silver WL (2018) The potential of agricultural land management to contribute to lower global surface temperatures. *Sci Adv* 4:aaq0932. <https://doi.org/10.1126/sciadv.aaq0932>
- Mayer LM (1994) Relationships between mineral surfaces and organic carbon concentrations in soils and sediments. *Chem Geol* 114:347–363. [https://doi.org/10.1016/0009-2541\(94\)90063-9](https://doi.org/10.1016/0009-2541(94)90063-9)
- Mayer LM, Schick LL, Hardy KR et al (2004) Organic matter in small mesopores in sediments and soils. *Geochim Cosmochim Acta* 68:3863–3872. <https://doi.org/10.1016/j.gca.2004.03.019>
- Mayer LM, Xing B (2001) Organic matter-surface area relationships in acid soils. *Soil Sci Soc Am J* 65:250–258. <https://doi.org/10.2136/sssaj2001.651250x>
- McCarthy JF, Ilavsky J, Jastrow JD et al (2008) Protection of organic carbon in soil microaggregates via restructuring of aggregate porosity and filling of pores with accumulating organic matter. *Geochim Cosmochim Acta* 72:4725–4744. <https://doi.org/10.1016/j.gca.2008.06.015>
- Mehra OP, Jackson ML (1958) Iron oxide removal from soils and clays by a dithionite-citrate system buffered with sodium bicarbonate. *Clays Clay Miner* 7:317–327. <https://doi.org/10.1346/ccmn.1958.0070122>
- Mikutta R, Kaiser K (2011) Organic matter bound to mineral surfaces: resistance to chemical and biological oxidation. *Soil Biol Biochem* 43:1738–1741. <https://doi.org/10.1016/j.soilbio.2011.04.012>
- Mikutta R, Kleber M, Kaiser K, Jahn R (2005) Review: organic matter removal from soils using hydrogen peroxide, sodium hypochlorite, and disodium peroxodisulfate. *Soil Sci Soc Am J* 69:120–135. <https://doi.org/10.2136/sssaj2005.0120>
- Mikutta R, Kleber M, Torn MS, Jahn R (2006) Stabilization of soil organic matter: association with minerals or chemical recalcitrance? *Biogeochemistry* 77:25–56. <https://doi.org/10.1007/s10533-005-0712-6>
- Mikutta R, Turner S, Schippers A et al (2019) Microbial and abiotic controls on mineral-associated organic matter in soil profiles along an ecosystem gradient. *Sci Rep* 9:10294. <https://doi.org/10.1038/s41598-019-46501-4>
- Moon J, Xia K, Williams MA (2019) Consistent proteinaceous organic matter partitioning into mineral and organic soil fractions during pedogenesis in diverse ecosystems. *Biogeochemistry* 142:117–135. <https://doi.org/10.1007/s10533-018-0523-1>
- Mueller CW, Kölbl A, Hoeschen C et al (2012) Submicron scale imaging of soil organic matter dynamics using NanoSIMS – From single particles to intact aggregates. *Org Geochem* 42:1476–1488. <https://doi.org/10.1016/j.orggeochem.2011.06.003>
- Mueller CW, Weber PK, Kilburn MR et al (2013) Advances in the analysis of biogeochemical interfaces: nanosims to investigate soil microenvironments. *Adv Agron* 121:1–46. <https://doi.org/10.1016/b978-0-12-407685-3.00001-3>
- Oades JM (1988) The retention of organic matter in soils. *Biogeochemistry* 5:35–70. <https://doi.org/10.1007/BF02180317>
- Ouberai MM, Xu K, Welland ME (2014) Effect of the interplay between protein and surface on the properties of adsorbed protein layers. *Biomaterials* 35:6157–6163. <https://doi.org/10.1016/j.biomaterials.2014.04.012>
- Plante AF, Conant RT, Stewart CE et al (2006) Impact of soil texture on the distribution of soil organic matter in physical and chemical fractions. *Soil Sci Soc Am J* 70:287–296. <https://doi.org/10.2136/sssaj2004.0363>
- Plaza C, Giannetta B, Benavente I et al (2019) Density-based fractionation of soil organic matter: effects of heavy liquid and heavy fraction washing. *Sci Rep* 9:10146. <https://doi.org/10.1038/s41598-019-46577-y>
- Possinger AR, Zachman MJ, Enders A et al (2020) Organo-organic and organo-mineral interfaces in soil at the nanometer scale. *Nat Commun* 11:6103. <https://doi.org/10.1038/s41467-020-19792-9>
- Ransom B, Bennett RH, Baerwald R, Shea K (1997) TEM study of in situ organic matter on continental margins: Occurrence and the “monolayer” hypothesis. *Mar Geol* 138:1–9. [https://doi.org/10.1016/S0025-3227\(97\)00012-1](https://doi.org/10.1016/S0025-3227(97)00012-1)
- RStudio Team (2020) RStudio: Integrated development for R. RStudio, PBC, Boston, MA URL. <http://www.rstudio.com>
- Scharlemann JPW, Tanner EVJ, Hiederer R, Kapos V (2014) Global soil carbon: understanding and managing the largest terrestrial carbon pool. *Carbon Manag* 5:81–91. <https://doi.org/10.4155/cmt.13.77>
- Schindelin J, Rueden CT, Hiner MC, Eliceiri KW (2015) The imagej ecosystem: an open platform for biomedical image analysis. *Mol Reprod Dev* 82:518–529. <https://doi.org/10.1002/mrd.22489>
- Schmidt MWI, Torn MS, Abiven S et al (2011) Persistence of soil organic matter as an ecosystem property. *Nature* 478:49–56. <https://doi.org/10.1038/nature10386>
- Schröder P, Huber B, Olazábal U et al (2002) Land use and sustainability: FAM research network on agroecosystems.

- Geoderma 105:155–166. [https://doi.org/10.1016/S0016-7061\(01\)00101-X](https://doi.org/10.1016/S0016-7061(01)00101-X)
- Schrumpf M, Kaiser K (2015) Large differences in estimates of soil organic carbon turnover in density fractions by using single and repeated radiocarbon inventories. *Geoderma* 239–240:168–178. <https://doi.org/10.1016/j.geoderma.2014.09.025>
- Schrumpf M, Kaiser K, Guggenberger G et al (2013) Storage and stability of organic carbon in soils as related to depth, occlusion within aggregates, and attachment to minerals. *Biogeosciences* 10:1675–1691. <https://doi.org/10.5194/bg-10-1675-2013>
- Schweizer SA, Bucka FB, Graf-Rosenfellner M, Kögel-Knabner I (2019) Soil microaggregate size composition and organic matter distribution as affected by clay content. *Geoderma* 355:113901. <https://doi.org/10.1016/j.geoderma.2019.113901>
- Schweizer SA, Hoeschen C, Schlüter S et al (2018) Rapid soil structure formation after glacial retreat driven by organic matter accrual at the microscale. *Global Change Biol* 24:1637–1650. <https://doi.org/10.1111/gcb.14014>
- Schwertmann U (1964) Differenzierung der Eisenoxide des Bodens durch Extraktion mit Ammoniumoxalat-Lösung. *J Plant Nutr Soil Sci* 105:194–202. <https://doi.org/10.1002/jpln.3591050303>
- Séquaris J-M, Guisado G, Magarinos M et al (2010) Organic-carbon fractions in an agricultural topsoil assessed by the determination of the soil mineral surface area. *J Plant Nutr Soil Sci* 173:699–705. <https://doi.org/10.1002/jpln.200800224>
- Six J, Conant RT, Paul EA, Paustian K (2002) Stabilization mechanisms of soil organic matter: implications for C-saturation of soils. *Plant Soil* 241:155–176. <https://doi.org/10.1023/a:1016125726789>
- Sollins P, Kramer MG, Swanston C et al (2009) Sequential density fractionation across soils of contrasting mineralogy: evidence for both microbial- and mineral-controlled soil organic matter stabilization. *Biogeochemistry* 96:209–231. <https://doi.org/10.1007/s10533-009-9359-z>
- Sollins P, Swanston C, Kleber M et al (2006) Organic C and N stabilization in a forest soil: evidence from sequential density fractionation. *Soil Biol Biochem* 38:3313–3324. <https://doi.org/10.1016/j.soilbio.2006.04.014>
- Sommer C, Strähle C, Köthe U, Hamprecht FA (2011) ilastik: Interactive Learning and Segmentation Toolkit 230–233
- Sommer M, Wehrhan M, Zipprich M et al (2003) Hierarchical data fusion for mapping soil units at field scale. *Geoderma* 112:179–196. [https://doi.org/10.1016/S0016-7061\(02\)00305-1](https://doi.org/10.1016/S0016-7061(02)00305-1)
- Steffens M, Rogge DM, Mueller CW et al (2017) Identification of distinct functional microstructural domains controlling c storage in soil. *Environ Sci Technol* 51:12182–12189. <https://doi.org/10.1021/acs.est.7b03715>
- Stewart CE, Paustian K, Conant RT et al (2007) Soil carbon saturation: concept, evidence and evaluation. *Biogeochemistry* 86:19–31. <https://doi.org/10.1007/s10533-007-9140-0>
- Stewart CE, Plante AF, Paustian K et al (2008) Soil carbon saturation: linking concept and measurable carbon pools. *Soil Sci Soc Am J* 72:379–392. <https://doi.org/10.2136/sssaj2007.0104>
- Stuiver M, Polach HA (1977) Discussion reporting of ^{14}C Data. *Radiocarbon* 19:355–363. <https://doi.org/10.1017/S003822200003672>
- Sulman BN, Moore JAM, Abramoff R et al (2018) Multiple models and experiments underscore large uncertainty in soil carbon dynamics. *Biogeochemistry* 141:109–123. <https://doi.org/10.1007/s10533-018-0509-z>
- Swanston CW, Torn MS, Hanson PJ et al (2005) Initial characterization of processes of soil carbon stabilization using forest stand-level radiocarbon enrichment. *Geoderma* 128:52–62. <https://doi.org/10.1016/j.geoderma.2004.12.015>
- Theng BKG, Ristori GG, Santi CA, Percival HJ (1999) An improved method for determining the specific surface areas of topsoils with varied organic matter content, texture and clay mineral composition. *Eur J Soil Sci* 50:309–316. <https://doi.org/10.1046/j.1365-2389.1999.00230.x>
- Torn MS, Trumbore SE, Chadwick OA et al (1997) Mineral control of soil organic carbon storage and turnover. *Nature* 389:170–173. <https://doi.org/10.1038/38260>
- Trumbore S (2009) Radiocarbon and soil carbon dynamics. *Annu Rev Earth Planet Sci* 37:47–66. <https://doi.org/10.1146/annurev.earth.36.031207.124300>
- Trumbore SE (1993) Comparison of carbon dynamics in tropical and temperate soils using radiocarbon measurements. *Global Biogeochem Cycles* 7:275–290. <https://doi.org/10.1029/93GB00468>
- von Lützw M, Kögel-Knabner I, Ekschmitt K et al (2007) SOM fractionation methods: relevance to functional pools and to stabilization mechanisms. *Soil Biol Biochem* 39:2183–2207. <https://doi.org/10.1016/j.soilbio.2007.03.007>
- Vos C, Jaconi A, Jacobs A, Don A (2018) Hot regions of labile and stable soil organic carbon in Germany – Spatial variability and driving factors. *SOIL* 4:153–167. <https://doi.org/10.5194/soil-4-153-2018>
- Wagai R, Mayer LM, Kitayama K (2009a) Extent and nature of organic coverage of soil mineral surfaces assessed by a gas sorption approach. *Geoderma* 149:152–160. <https://doi.org/10.1016/j.geoderma.2008.11.032>
- Wagai R, Mayer LM, Kitayama K (2009b) Nature of the “occluded” low-density fraction in soil organic matter studies: A critical review. *Soil Sci Plant Nutr* 55:13–25. <https://doi.org/10.1111/j.1747-0765.2008.00356.x>
- Wang X, Toner BM, Yoo K (2019) Mineral vs. organic matter supply as a limiting factor for the formation of mineral-associated organic matter in forest and agricultural soils. *Sci Total Environ* 692:344–353. <https://doi.org/10.1016/j.scitotenv.2019.07.219>
- Weller U, Zipprich M, Sommer M et al (2007) mapping clay content across boundaries at the landscape scale with electromagnetic induction. *Soil Sci Soc Am J* 71:1740. <https://doi.org/10.2136/sssaj2006.0177>

Wiseman CLS, Puttmann W (2005) Soil organic carbon and its sorptive preservation in central Germany. *Eur J Soil Science* 56:65–76. <https://doi.org/10.1111/j.1351-0754.2004.00655.x>

Zhong Z, Chen Z, Xu Y et al (2018) Relationship between soil organic carbon stocks and clay content under different

climatic conditions in central China. *Forests* 9:598. <https://doi.org/10.3390/f9100598>

Publisher's Note Springer Nature remains neutral with regard to jurisdictional claims in published maps and institutional affiliations.